SAGE ICRP

New mesh-type phantoms and their dosimetric applications, including emergencies

C.H. Kim[a], Y.S. Yeom[a], T.T. Nguyen[a], M.C. Han[a], C. Choi[a], H. Lee[a], H. Han[a], B. Shin[a], J-K. Lee[a], H.S. Kim[b], M. Zankl[c], N. Petoussi-Henss[c], W.E. Bolch[d], C. Lee[e], B.S. Chung[f], R. Qiu[g], K. Eckerman[h]

[a]*Department of Nuclear Engineering, Hanyang University, 04763, 222 Wangsimni-ro, Seongdong-gu, Seoul, Republic of Korea; e-mail: chkim@hanyang.ac.kr*
[b]*Korea Institute of Radiological & Medical Sciences, Republic of Korea*
[c]*Helmholtz Zentrum München Deutsches Forschungszentrum für Gesundheit und Umwelt, Germany*
[d]*University of Florida, USA*
[e]*National Cancer Institute, USA*
[f]*Ajou University School of Medicine, Republic of Korea*
[g]*Tsinghua University, P.R. China*
[h]*Oak Ridge National Laboratory, USA*

Abstract–Committee 2 of the International Commission on Radiological Protection (ICRP) has constructed mesh-type adult reference computational phantoms by converting the voxel-type ICRP *Publication 110* adult reference computational phantoms to a high-quality mesh format, and adding those tissues that were below the image resolution of the voxel phantoms and therefore not included in the *Publication 110* phantoms. The new mesh phantoms include all the necessary source and target tissues for effective dose calculations, including the 8–40-μm-thick target layers of the alimentary and respiratory tract organs, thereby obviating the need for supplemental organ-specific stylised models (e.g. respiratory airways, alimentary tract organ walls and stem cell layers, lens of the eye, and skin basal layer). To see the impact of the new mesh-type reference phantoms, dose coefficients for some selected external and internal exposures were calculated and compared with the current reference values in ICRP *Publications 116* and *133*, which were calculated by employing the *Publication 110* phantoms and the supplemental stylised models. The new mesh phantoms were also used to calculate

This paper does not necessarily reflect the views of the International Commission on Radiological Protection.

dose coefficients for industrial radiography sources near the body, which can be used to estimate the organ doses of the worker who is accidentally exposed by an industrial radiography source; in these calculations, the mesh phantoms were deformed to reflect the size of the worker, and also to evaluate the effect of posture on dose coefficients.

Keywords: Reference ICRP phantom; Voxel-type phantom; Mesh-type phantom; Monte Carlo; Dose coefficient

1. INTRODUCTION

Following the issuance of the 2007 Recommendations of the International Commission on Radiological Protection (ICRP) (ICRP, 2007), the Commission released the ICRP adult reference computational phantoms with *Publication 110* (ICRP, 2009). These *Publication 110* reference phantoms are voxel-type computational phantoms that were constructed from the whole-body computed tomography (CT) data of adult male and female patients. They are consistent with the information in *Publication 89* (ICRP, 2002), the reference anatomical parameters of Reference Adult Male and Reference Adult Female. The voxel-type *Publication 110* reference phantoms have been used to produce reference dose coefficients (DCs) of equivalent and effective doses for external and internal exposures, following the current ICRP dosimetric framework (ICRP, 2010, 2015, 2016, 2017).

While providing anatomically more realistic representations of the human body than the first-generation computational phantoms (i.e. stylised or mathematical phantoms), the voxel-type *Publication 110* reference phantoms (ICRP, 2009), due to millimetre-scale voxel resolutions (male: $2.137 \times 2.137 \times 8.0\,\mathrm{mm}^3$; female: $1.775 \times 1.775 \times 4.84\,\mathrm{mm}^3$), do not include small or thin tissues, particularly micron-scale radiosensitive target layers (e.g. the stem cell layers of respiratory and alimentary tract organs and the skin basal layer), eventually leading to limitations in DC calculations for weakly penetrating radiations (i.e. low-energy photons and charged particles). Therefore, several supplemental organ-specific stylised models were developed and used for separate simulations to calculate reference DCs for some exposure cases, for which the *Publication 110* phantoms would not provide reliable dose values (ICRP, 2010, 2015, 2016, 2017). In addition, due to the nature of voxel geometry, it is very difficult, if not impossible, to deform the *Publication 110* reference phantoms into different body sizes or postures, which is needed for personalisation of dose calculations in emergency or accident exposure situations.

Acknowledging these limitations, the Commission has recently launched Task Group 103 under Committee 2 with the aim of developing new mesh-type reference computational phantoms (MRCPs) by converting the current voxel-type reference phantoms into a high-quality mesh format. Note that these mesh-type phantoms, represented by polygon mesh (PM) or tetrahedral mesh (TM) as necessary, are considered, at present, as an advanced type of computational phantom that can be

implemented directly into Monte Carlo codes (i.e. without voxelisation), fully maintaining the advantages of the mesh geometry over the voxel geometry in Monte Carlo dose calculations (Kim et al., 2011; Han et al., 2013, 2015; Yeom et al., 2013, 2014). Very recently, Task Group 103 completed the development of the MRCPs for adult male and female, converted from the voxel-type *Publication 110* reference phantoms (Nguyen et al., 2015; Kim et al., 2016; Yeom et al., 2016a,b; Kim et al., 2017).

This paper introduces the new adult MRCPs, with a brief explanation of the development process, and discusses their compatibility with some major general-purpose Monte Carlo codes and the impact on DC calculations. In addition, the first application of the MRCPs by Task Group 103 is explained, which is the calculation of DCs for industrial radiography sources for use in dose estimation of workers who are accidentally exposed by an industrial radiography source.

2. ADULT MESH-TYPE REFERENCE PHANTOMS

Most of the organs and tissues of the adult MRCPs were constructed by directly converting the voxel-type *Publication 110* reference phantoms (ICRP, 2009) into mesh format through three-dimensional surface rending and several refinement procedures (Kim et al., 2016). During the conversion process, the shape of each organ/tissue of the mesh model was matched to the voxel model, maximising the geometric similarity between two objects, which was monitored by the Dice index (DI) (Dice, 1945) and centroid distance (CD). The direct conversion method was also used to construct the bones, except for some bones such as the spine, hand, and foot bones which were constructed from existing high-quality mesh models by morphing, again monitoring the DI and CD. Detailed information on construction of the skeletal system can be found elsewhere (Yeom et al., 2016b).

Several organs and tissues (e.g. small intestine, lymphatic nodes, eye, and blood in large vessels), which are very complex and/or small in structure, could not be produced by the conversion process; therefore, they were modelled. The small intestine of each phantom was generated using a dedicated procedure and a computer program developed by Yeom et al. (2016a), in which a total of 1000 different models of the small intestine are generated randomly with a Monte Carlo approach, and then the best model is selected considering both geometric and dosimetric similarity with the *Publication 110* phantoms (ICRP, 2009). The lymphatic nodes were generated using a similar approach, which was used to generate the lymphatic nodes in the University of Florida and the National Cancer Institute (UF/NCI) adult phantoms (Lee et al., 2013), based on the lymphatic node data in *Publication 133* (ICRP, 2016). The detailed eye model, which was developed by Behrens et al. (2009) and adopted to calculate the lens DCs in *Publication 116* (ICRP 2010), was reproduced in high-quality mesh format and installed in the MRCPs (Nguyen et al., 2015). The blood in the large vessels (Fig. 1) was modelled considering the distribution of the blood in the voxel phantoms and the shape of the three-dimensional blood models in BioDigital (https://www.biodigital.com), and also matching the mass to the reference

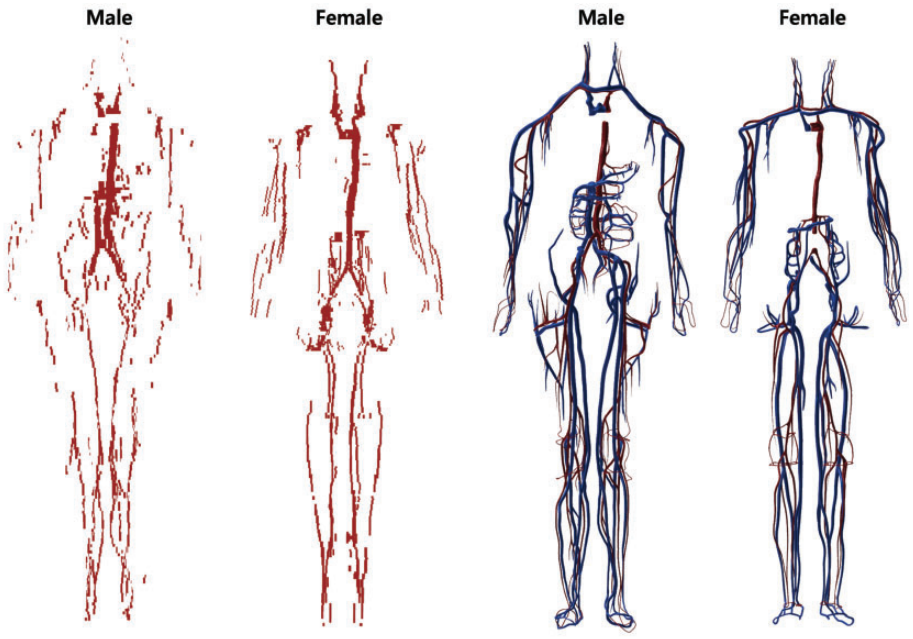

Fig. 1. Blood in large vessels of the *Publication 110* phantoms (ICRP, 2009) (left) and the mesh-type reference computational phantoms (MRCPs) (right). In the MRCPs, the red colour indicates the blood in the large arteries and the blue colour indicates the blood in the large veins.

value given in *Publication 89* (ICRP, 2002). The constructed models were finally reviewed and confirmed by an anatomist.

The *Publication 110* phantoms (ICRP, 2009), as well as the other previous computational phantoms (Kramer et al., 1982, 2006; Zankl et al., 2005; Lee et al., 2007, 2010; Zhang et al., 2009; Yeom et al., 2013), were matched to the reference organ/tissue masses listed in Table 2.8 of *Publication 89* (ICRP, 2002), which are the parenchyma masses of the organs and tissues (i.e. not including blood content). It is true that a large portion of blood situated in the small vessels and capillaries is distributed in the organs and tissues; therefore, the MRCPs were adjusted to the organ/tissue masses and compositions which are inclusive of the blood content. For this, the organ/tissue masses and compositions were recalculated following the reference regional blood volume fractions in *Publication 89* (ICRP, 2002). Note that a similar approach has been used for the calculation of specific absorbed fractions (SAFs) for the self-irradiation cases in *Publication 133* (ICRP, 2016).

Micron-thick target and source regions of the skin and respiratory and alimentary tract organs were included in the MRCPs. The 50-μm-thick skin basal cell layer (i.e. 50–100 μm below the skin surface), recommended by the Commission (ICRP, 1977, 2010, 2015), was defined in the MRCPs, as shown in Fig. 2, simply by using the

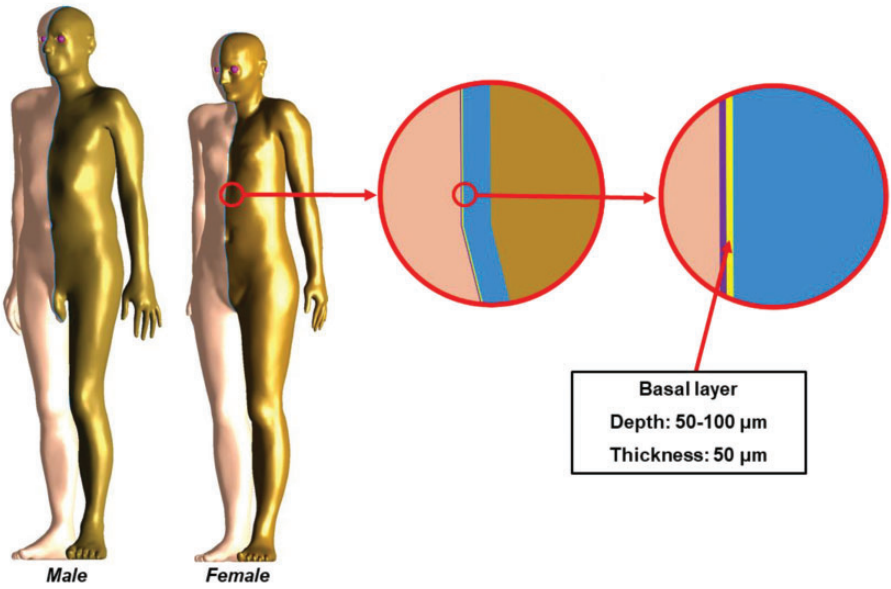

Fig. 2. Skin of the adult mesh-type reference computational phantoms including the 50-μm-thick target layer: dead layer (purple), target layer (yellow), and dermis layer (blue).

'offset' function that shrinks or enlarges a polygon-mesh surface in the normal directions of the facets of the surface, which allows the creation of surfaces to define the tens-of-micrometres-thick layer at a specific depth. Likewise, the thin target and source regions of the respiratory tract organs (extrathoracic region, bronchi, bronchioles, and alveoli-interstitial region) and the alimentary tract organs (oral cavity, oesophagus, stomach, small intestine, and colon) were defined in the MRCPs, following the morphometric data given in *Publications 66* and *100* (ICRP, 1994, 2006). Detailed lung airway models to represent the bronchi and bronchioles were also developed using the branch generation algorithm of Tawhai et al. (2000), as shown in Fig. 3. More detailed information on the respiratory and alimentary tract systems can be found elsewhere (Kim et al., 2017).

Fig. 4 shows the adult male and female MRCPs, along with the voxel-type *Publication 110* reference phantoms (ICRP, 2009). The body height and weight of the MRCPs exactly match the reference values (male: 176 cm and 73 kg; female: 163 cm and 60 kg). The masses of the organs and tissues of the MRCPs match the reference values, inclusive of blood content, within 0.1% of the difference. The male MRCP is composed of 2.5 million triangular facets in the PM format and 8.2 million tetrahedrons in the TM format. The female MRCP is composed of 2.6 million triangular facets in the PM format and 8.6 million tetrahedrons in the TM format. Note that the TM-version MRCPs were converted directly from the PM-version MRCPs without any geometric distortion using the TetGen code (Si, 2015). The

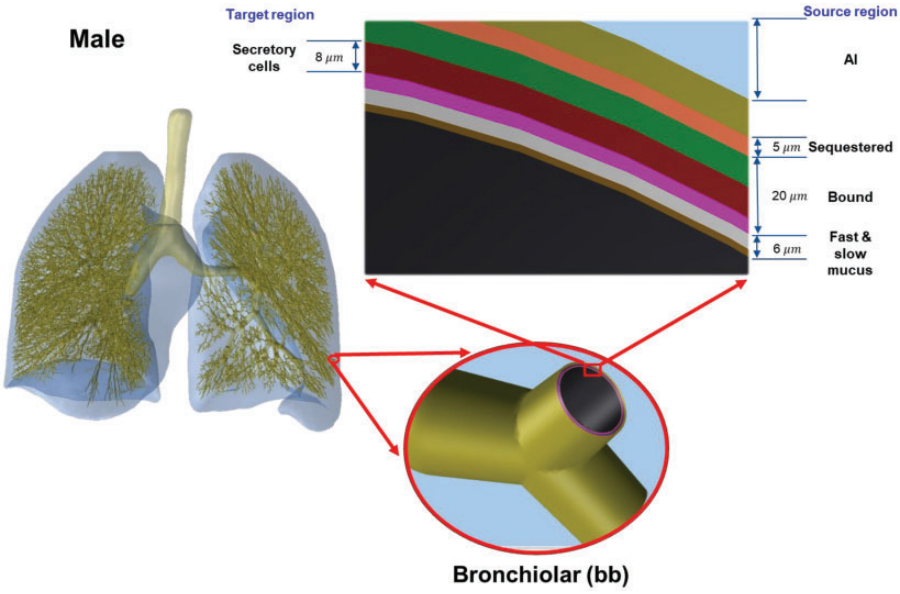

Fig. 3. Detailed airway model incorporated in the lungs of the adult male mesh-type reference computational phantom (Kim et al., 2017).

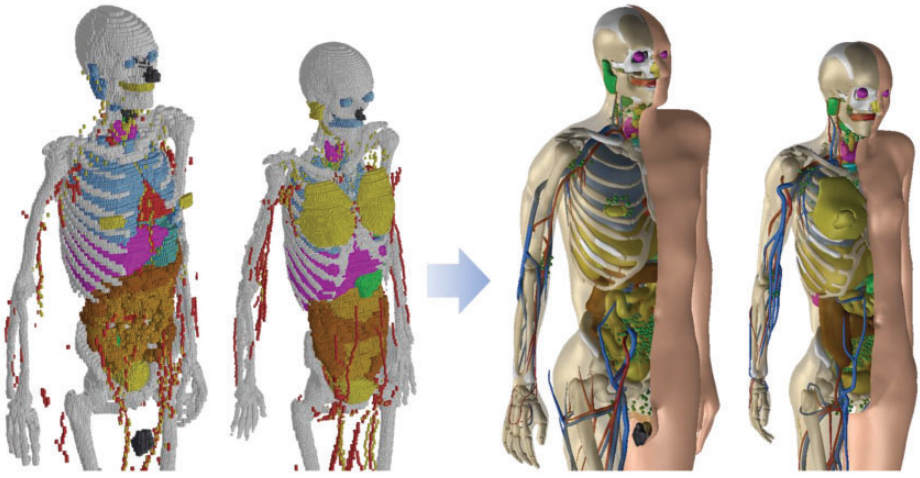

Fig. 4. The adult mesh-type reference phantoms (MRCPs) (right), along with the voxel-type ICRP *Publication 110* reference phantoms (ICRP, 2009) (left). Note that the MRCPs are constructed in polygon-mesh format, but changed to tetrahedral-mesh format when these are used in Monte Carlo codes in order to increase computation speed.

MRCPs include all the radiosensitive organs and tissues relevant to the dose assessment for ionising radiation exposure for radiological protection purposes, thereby completely obviating the need for supplemental organ-specific stylised models such as respiratory airways, alimentary tract organ walls and stem cell layers, lens of the eye, and skin basal cell layer. Due to the complexity of the structures, the red bone marrow and endosteum are not explicitly modelled in the MRCPs, and the doses to these tissues need to be estimated by using the skeletal dose calculation methods (e.g. fluence-to-dose–response functions), as in *Publication 116* (ICRP, 2010). Note that the lung airway models, representing bronchi and bronchioles, were produced in the constructive solid geometry format, not in mesh format, and can be installed in the MRCPs, as necessary, using the Geant4 code via the parallel-geometry technique (Apostolakis et al., 2008; Kim et al., 2017). The MRCPs have overcome the geometrical limitations of the *Publication 110* phantoms (ICRP, 2009) due to the limited voxel resolutions and the nature of voxel geometry. For example, as shown in Fig. 4, the *Publication 110* phantoms show stair-stepped surfaces of the organs and tissues, whereas the MRCPs show smooth surfaces. In addition, all the organs and tissues in the thin structure (e.g. skin, gastrointestinal tract organs, and cortical bone) are represented discontinuously in the *Publication 110* phantoms (ICRP, 2009; Yeom et al., 2013, 2016b), and represented continuously in the MRCPs.

3. COMPATIBILITY WITH MONTE CARLO CODES

The major Monte Carlo radiation transport codes, such as Geant4, MCNP6, PHITS, and FLUKA, can directly implement PM or TM geometries. The Geant4 code can implement both PM and TM geometries by using 'G4TessellatedSolid' class and 'G4Tet' class, respectively (Agostinelli et al., 2003). The MCNP6 code, as a merger of MCNP5 and MCNPX capabilities, provides the unstructured mesh geometry which can implement the TM geometries. Note that since Version 1.1 beta of the MCNP6, the unstructured mesh geometry has been able to support the transport of most particles available in the MCNP6 code (Goorley et al., 2013), whereas in the previous version (i.e. Version 1.0), the transport of neutrons and gamma rays alone was supported (Martz et al., 2012). The PHITS code, since Version 2.82, can implement TM geometries (Sato et al., 2013). Note that nowadays, the PHITS code is used predominantly by ICRP to calculate DCs. The FLUKA code can implement the PM geometry via FluDAG (http://svalinn.github.io/DAGMC-/index.html).

Memory usage and computation speed were measured for Geant4 (Version 10.03 patch01), MCNP6 (Version 2.0 pre-release), and PHITS (Version 2.92) when the male MRCP in the TM format was used in Monte Carlo dose calculation. For this, the MRCP was directly implemented into the Monte Carlo codes as shown in Fig. 5. The phantom was then irradiated in the isotropic irradiation geometry. The primary particles considered are photons (10^{-2}–10^{4} MeV), electrons (10^{-2}–10^{4} MeV), neutrons (10^{-8}–10^{4} MeV), and helium ions (1–10^{5} MeV/u). To evaluate the computation speed, the computation time was measured by simulating 10^{5} primary

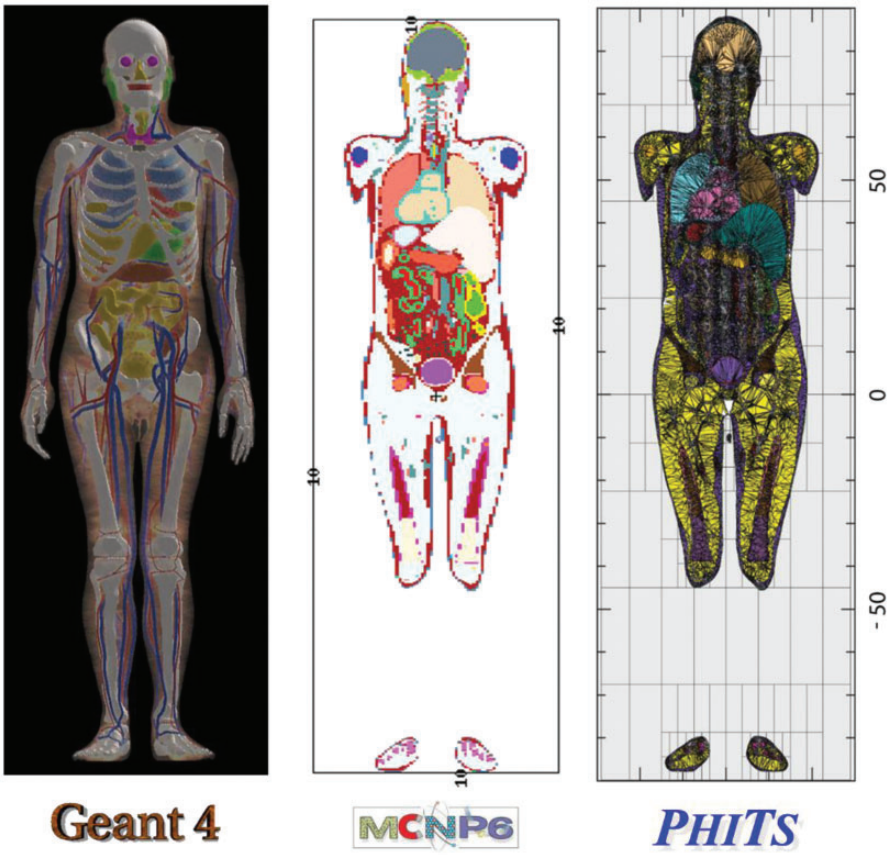

Fig. 5. The adult male mesh-type reference computational phantom implemented in Geant4 (left), MCNP6 (middle), and PHITS (right).

particles. For the Geant4 code, the physics libraries of 'G4EmLivermorePhysics' and 'FTFP_BERT_HP' were used to transport all the particles. In addition, the thermal neutron scattering treatment $S(\alpha, \beta)$ for H in light water at 300 K was applied for precise transport of thermal neutrons. A default range of 1 mm for the secondary production cut was applied to all the particles. For both the MCNP6 code and the PHITS code, the default physics models and cross-section data were used to transport all the particles, and the thermal neutron scattering treatment was also applied. For the MCNP6 code, the default cut energies were used, which were also applied to set cut energies for the PHITS code. The simulations were performed on a single core of Intel Xeon CPU E5-2698 Version 4 (2.20 GHz CPU processors and 512 GB memory).

First, memory usage was measured for the three Monte Carlo codes. The Geant4 code required approximately 11 GB, which is slightly less than that required by the

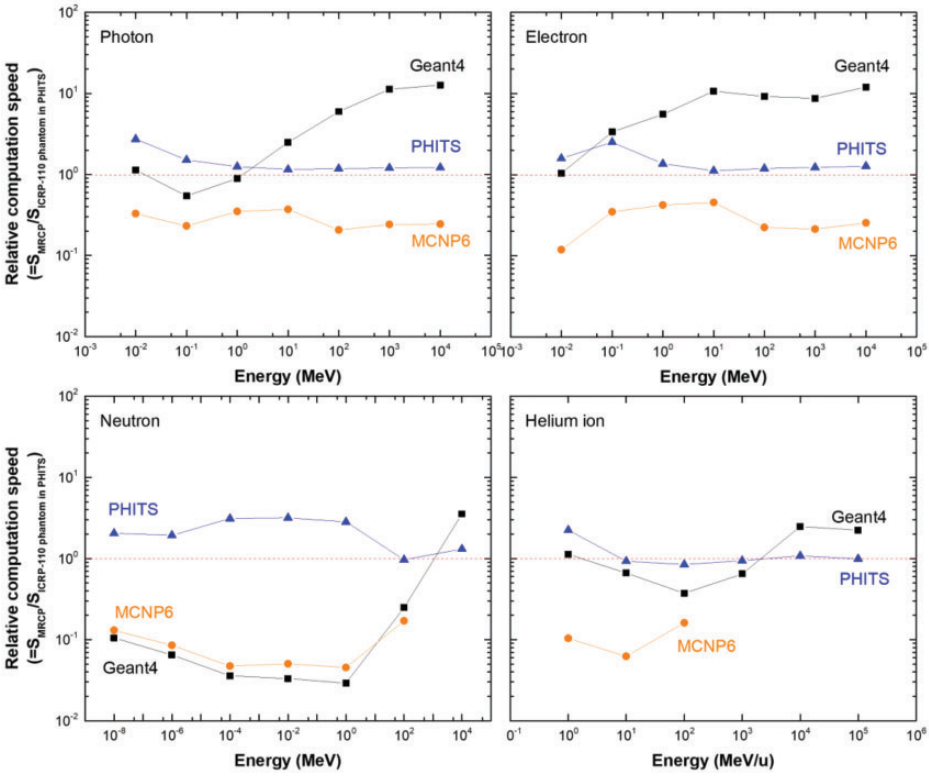

Fig. 6. Relative computation speed of the adult male mesh-type reference computational phantom on Geant4, MCNP6, and PHITS, with respect to the computation speed of the *Publication 110* male phantom on the PHITS code.

MCNP6 code (approximately 14 GB). The PHITS code, when compared with the other codes, required much less memory (approximately 1.2 GB), which is because the PHITS code uses dynamic allocation for most of the memory needed for implementing the MRCP. Considering the memory usages, all of the Monte Carlo codes can be used for dose calculations with the MRCPs on a personal computer, needing a maximum of 64 GB. In addition, initialisation times were measured for the three Monte Carlo codes, which were all less than a few minutes, negligibly contributing to the total computation time of typical DC calculations requiring several hours or tens of hours depending on particles and energies (Furuta et al., 2017).

Computation speed of the MRCP on the three Monte Carlo codes was measured and then compared with that measured with the *Publication 110* male phantom (ICRP, 2009) on the PHITS code. Again, note that nowadays, ICRP calculates most DCs using the *Publication 110* phantoms and the PHITS code. Fig. 6 shows the relative computation speed of the adult male MRCP on the three Monte Carlo codes, with respect to the computation speed of the *Publication 110* phantom on the

PHITS code (= the ratio of the MRCP computation speed on the Monte Carlo codes to the computation speed of the *Publication 110* phantom on the PHITS code). First of all, it can be seen that the relative computation speed of the MRCP on the PHITS code is generally greater than unity, which means that the computation speed of the MRCP is generally faster than that of the *Publication 110* phantom on the PHITS code. This result is very encouraging and implies that, assuming that ICRP keeps using the PHITS code for most DC calculations, the use of MRCPs will improve the computation speed of DCs. For the Geant4 code, the computation speed of the MRCP is faster or comparable to that of the *Publication 110* phantom on the PHITS code for photons, electrons, and helium ions. For neutrons, however, with an exception at 10^4 MeV, the computation speed of the MRCP is much slower (i.e. more than 30 times slower; 1 MeV). For the MCNP6 code, for all the cases considered, the computation speed of the MRCP is much slower than that of the *Publication 110* phantom on the PHITS code (i.e. by a factor of 2–22). This seems mainly due to the fact that the MCNP6 code uses the unstructured mesh geometry, which is very flexible but overly sophisticated to define the simple TM geometry. The authors believe that the computation speed will improve if the MCNP6 code uses a dedicated geometry for TM geometry in the future.

4. COMPARISON OF DOSE COEFFICIENTS

In order to evaluate the impact of the adult MRCPs in dose calculations, DCs were calculated for some selected external and internal exposure cases, and the calculated DCs were compared with the current reference values in *Publications 116* and *133* (ICRP, 2010, 2016) that were produced using the *Publication 110* (ICRP, 2009) phantoms and the stylised models adopted in the previous publications (ICRP, 1994, 2006, 2015, 2016, 2017). For this, the MRCPs were implemented directly into the Geant4 code. Similar to the calculations of the computation speeds, the physics libraries of 'G4EmLivermorePhysics' and 'FTFP_BERT_HP' were used with the thermal neutron scattering treatment, but the default range of 1 mm for the secondary production cut was changed to 1 μm for more precise dose calculations. For external exposures, the effective DCs in terms of effective dose per fluence (in pSv cm^2) were calculated for mono-energetic broad parallel beams of photons, neutrons, electrons, and helium ions for the same irradiation geometries considered in *Publication 116* (ICRP, 2010). For internal exposures, the effective doses per radiation emission for photons and electrons were calculated for selected source organs/tissues: the cortical bone, liver, lungs, and thyroid. Note that the effective dose per radiation emission is the expected value of the effective dose resulting from an emission of a single radiation particle in a source organ/tissue, which is calculated from SAFs and the radiation and tissue weighting factors of *Publication 103* (ICRP, 2007). The statistical errors of the calculated values were all less than 0.5%.

The calculation results showed that, for photons and neutrons, the MRCPs tended to provide very similar DC values for both organ/tissue doses and effective doses to the reference values in *Publications 116* and *133* (ICRP, 2010, 2016) for both

external and internal exposures. The differences in the effective doses, the most important protection quantity, were even smaller than those in the organ/tissue doses. For photons, for example, with some exceptions at low energies (<0.03 MeV), the effective dose differences were less than 2% for external exposures and less than 5% for internal exposures. For neutrons, for which only external exposures were considered, the differences were larger due to the different Monte Carlo codes used in the calculations, but still less than 10% for most external exposure cases. Note that for neutrons, the *Publication 116* values were calculated using several different codes such as MCNPX, PHITS, FLUKA, and Geant4 (ICRP, 2010). For charged particles (i.e. electrons and helium ions), in contrast, the MRCPs tended to provide different values from the *Publication 116* and *133* values for the organ/tissue DCs and SAFs for both external and internal exposures. For the effective doses, however, with some exceptions, the differences were generally not very large (i.e. less than approximately 5% for most cases for both external and internal exposures).

The exceptions were found in the results of external exposures by electrons (<1 MeV) and helium ions (<10 MeV u^{-1}). Fig. 7 shows an example of the effective DCs for electron exposures in the antero-posterior irradiation geometry. It can be seen that the effective DCs of the MRCPs are very similar to those in *Publication 116* (ICRP, 2010) for energies higher than 1 MeV, but for the lower energies, there are large differences; the maximum difference is as much as approximately 7000 times at

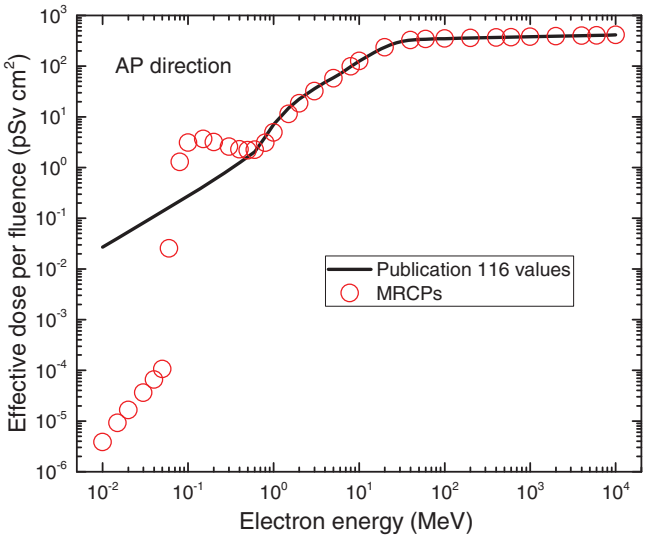

Fig. 7. Effective dose per fluence (pSv cm^2) calculated with the adult mesh-type reference computational phantoms (MRCPs) (red circles) and the *Publication 116* (ICRP, 2010) values (black line) for electron exposures in the antero-posterior (AP) irradiation geometry.

the lowest energy. These differences are mostly influenced by differences in the skin DCs, which are mainly caused by use of the 50-μm-thick skin target layer in the MRCPs. It should be noted that the *Publication 110* phantoms (ICRP, 2009) do not have the 50-μm-thick skin target layer due to the millimetre-order voxel resolutions; therefore, the *Publication 116* skin DCs were calculated by averaging absorbed dose over the entire skin of the phantom, instead of the thin skin target layer. The same level of differences was also found in the results of the other irradiation geometries, although they are not presented in the figure.

However, it is also true that the differences are overly exaggerated by considering mono-energetic electron beams alone; in real exposure situations, generally polyenergetic electrons (e.g. beta spectrum) are involved, where the difference in effective doses is less significant. For example, the difference of effective dose between the MRCPs and the *Publication 110* phantoms (ICRP, 2009), resulting from the antero-posterior irradiation of the beta radiation sources (^{14}C, ^{186}Re, ^{32}P, ^{90}Sr/^{90}Y, and ^{106}Rh), is less than approximately two times, except for ^{14}C, for which the difference is approximately five times. Note that although ^{14}C shows relatively large differences, it emits very low energy electrons (0.15 MeV maximum), and thus is generally not of concern for external exposures.

5. CALCULATION OF DOSE COEFFICIENTS FOR INDUSTRIAL RADIOGRAPHY SOURCES

Using the adult MRCPs, Task Group 103 is currently calculating DCs for industrial radiography sources, which can be used to estimate organ/tissue and effective doses of workers who are accidentally exposed to an industrial radiography source. According to the International Atomic Energy Agency (IAEA, 2011), accidents involving industrial radiography sources result in very high radiation doses to workers, causing serious injuries and, in a few cases, even death. IAEA (1998) states that industrial radiography accounts for approximately half of all the reported accidents for the nuclear-related industry in both developed and developing countries.

For the DC calculations, ^{192}Ir and ^{60}Co industrial radiography sources were assumed as a point source and modelled near the MRCPs. The point sources are located at three distances (0.5, 10, and 30 cm) in four directions (front, back, right, and left) at five levels (ground, mid thigh, lower torso, mid torso, and upper torso) (see Fig. 8). In addition, three longer distances (100, 150, and 300 cm) are considered in the four directions at the lower torso level. The source distance used in the calculations is the distance from the surface of the phantom, except for the front and back directions at the ground and mid thigh levels, for which the distance is calculated from the centre of the imaginary segment tangent to the surfaces of the left and right legs at the given level. Organ/tissue DCs (= absorbed dose per disintegration) for red bone marrow, brain, lungs, small intestine, and colon are calculated,

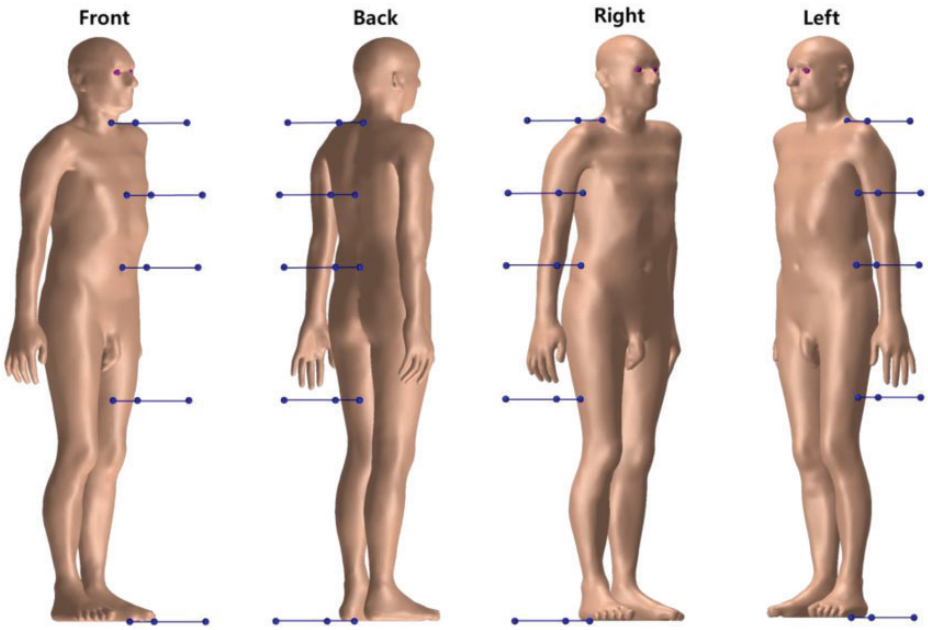

Fig. 8. Source locations at three distances (0.5, 10, and 30 cm) at five levels (ground, mid thigh, lower torso, mid torso, and upper torso) in four directions (front, back, right, and left).

considering acute radiation syndromes. Effective DCs (= effective dose per disintegration) are also calculated for comparison purposes.

In addition to the MRCPs, the 10th and 90th percentile phantoms are also employed in the DC calculations to consider the influence of different body sizes on DCs. Fig. 9 shows the 10th and 90th percentile male phantoms, along with the adult male MRCP. The 10th percentile phantom, which represents a very small person, was constructed by reducing the size of the MRCPs to the 10th percentile standing height and 10th percentile body mass in the Caucasian population. In contrast, the 90th percentile phantom, which represents a very large person, was constructed by increasing the size of the MRCPs to the 90th percentile standing height and 90th percentile body mass. For the constructions, the standing height and body mass percentiles were derived from the data of the nine countries (i.e. Sweden, Netherlands, Germany, Belgium, Australia, USA, France, UK, and Italy) provided in the PeopleSize commercial software (www.openerg.com). Additional anthropometric parameters (i.e. head height; length and breadth; upper arm, waist, buttock, thigh and calf circumferences; waist depth; and sitting height), corresponding to the standing height and body mass percentiles, were derived not only from the PeopleSize data, but also from the National Health and Nutrition

Fig. 9. Computational phantoms: 10th percentile phantom (left), mesh-type reference computational phantom (middle), and 90th percentile phantom (right) for adult males.

Examination Survey (https://www.cdc.gov/nchs/nhanes/index.htm) and the US Army Anthropometric Survey (Gordon et al., 2014) databases. A complete set of the DCs of the MRCPs and the 10th and 90th percentile phantoms will be provided in the Task Group 103 report for the adult MRCPs. Additionally, the effect of different postures will be investigated by calculating DCs with several phantoms with different postures (i.e. walking, sitting, bending, kneeling, and squatting postures), which are now under construction by deforming the MRCPs. For the investigation, the DCs will be calculated for the lowest-energy source, ^{192}Ir, located 100 cm from the phantom surface in the four directions at the lower torso level.

Fig. 10 shows, as an example, the small intestine DCs of the adult male MRCP, along with those of the 10th and 90th percentile adult male phantoms, for the ^{192}Ir source located in the four directions at the lower torso level. It can be seen that body size significantly influences the DC values. The DC of the 90th percentile phantom is smaller than that of the MRCP by up to 2.6 times (at 0.5 cm in the front direction). On the other hand, the DC of the 10th percentile phantom is larger by up to approximately 40% (at 0.5 cm in the front direction).

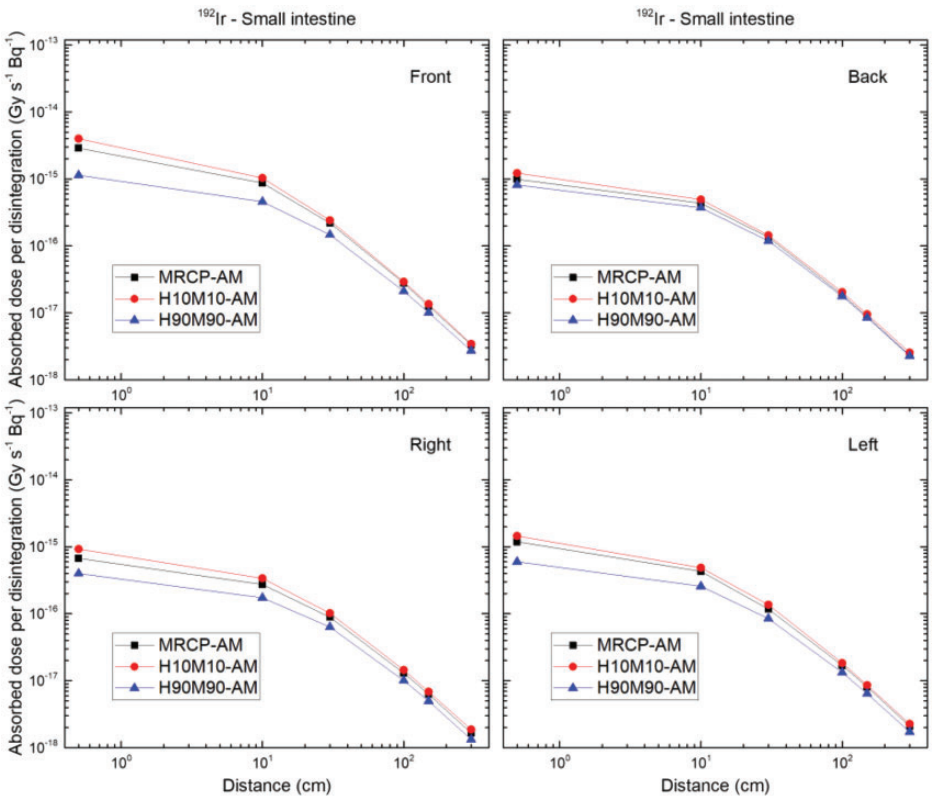

Fig. 10. Small intestine dose coefficients of the adult male mesh-type reference computational phantom (MRCP) (black squares) for a point source of ^{192}Ir as a function of the distance from the surface of the phantom in the four directions (front, back, right, and left) at the lower torso level, along with those of the 10th percentile adult male phantom (red circles), and the 90th percentile adult male phantom (blue triangles).

6. CONCLUSIONS

Task Group 103 of ICRP Committee 2 has completed the adult male and female MRCPs to address the limitations of the current voxel-type *Publication 110* reference phantoms (ICRP, 2009) due to the low voxel resolutions and the nature of voxel geometry. The adult MRCPs were constructed by converting the *Publication 110* phantoms into the high-quality mesh format, also including all the necessary source and target tissues for effective dose calculations (e.g. the 8–40-μm-thick target layers of the alimentary and respiratory tract organs), thereby obviating the need for supplemental organ-specific stylised models (e.g. respiratory airways, alimentary tract organ walls and stem cell layers, lens of the eye, and skin basal layer). The compatibility of the MRCPs with the three major general purpose Monte Carlo

codes (Geant4, MCNP6, and PHITS) was investigated by measuring memory usage and computation speed, especially finding that the MRCPs are even faster than the current *Publication 110* phantoms in the PHITS code, which is used by ICRP nowadays for most DC calculations. The dosimetric impact of the MRCPs was also investigated by calculating some external and internal DCs, which were then compared with the current reference values in *Publications 116* and *133* (ICRP, 2010, 2016); the results showed that the MRCPs tend to provide very similar DC values for highly penetrating radiations (e.g. photons and neutrons), while providing more reliable DC values for weakly penetrating radiations (e.g. electrons and helium ions). In addition, Task Group 103 is currently calculating the DCs for industrial radiography sources; in these calculations, the MRCPs are deformed to reflect the size of individuals, and also to evaluate the effect of the posture on DCs, which demonstrates the capability of the MRCPs in individualised dose calculations. Acknowledging the advantages, Committee 2 is planning to use the MRCPs in the calculation of DCs for emergency exposure situations, which is planned for the next term (2017–2020). The Task Group 103 report is now under preparation in order to officially release the adult MRCPs; the report is expected to be published in 2019, after public consultation in 2018.

REFERENCES

Agostinelli, S., Allison, J., Amako, K., et al., 2003. GEANT4 – a simulation toolkit. Nucl. Instr. Meth. Phys. Res. A 506, 250–303.

Apostolakis, J., Asai, M., Cosmo, G., et al., 2008. Parallel geometries in Geant4: foundation and recent enhancements. Proceedings of the IEEE NSS/MIC/RTSD Conference, 19–25 October 2008, Dresden, Germany.

Behrens, R., Dietze, G., Zankl, M., 2009. Dose conversion coefficients for electron exposure of the human eye lens. Phys. Med. Biol. 54, 4069–4087.

Dice, L.R., 1945. Measures of the amount of ecologic association between species. Ecology 26, 297–302.

Furuta, T., Sato, T., Han, M.C., et al., 2017. Implementation of tetrahedral-mesh geometry in Monte Carlo radiation transport code PHITS. Phys. Med. Biol. 62, 4798–4810.

Goorley, J.T., James, M.R., Booth, T.E., et al., 2013. Initial Mcnp6 Release Overview-Mcnp6 Version 1.0. No. LA-UR-13-22934. Los Alamos National Laboratory, Los Alamos, NM.

Gordon, C.C., Blackwell, C.L., Bradtmiller, B., et al., 2014. 2012 Anthropometric Survey of U.S. Army Personnel: Methods and Summary Statistics. NATICK/TR-15/007. US Army Natick Soldier Research, Development, and Engineering Center, Natick, MA.

Han, M.C., Kim, C.H., Jeong, J.H., et al., 2013. Dagsolid: a new Geant4 solid class for fast simulation in polygon-mesh geometry. Phys. Med. Biol. 58, 4595–4609.

Han, M.C., Yeom, Y.S., Kim, C.H., et al., 2015. New approach based on tetrahedral-mesh geometry for accurate 4d Monte Carlo patient-dose calculation. Phys. Med. Biol. 60, 1601–1612.

IAEA, 1998. Lessons Learned from Accidents in Industrial Radiography. Safety Reports Series No. 7. International Atomic Energy Agency, Vienna.

IAEA, 2011. Radiation Safety in Industrial Radiography. IAEA Safety Standards Series No. SSG-11. International Atomic Energy Agency, Vienna.

ICRP, 1977. Recommendations of the ICRP. ICRP Publication 26. Ann. ICRP 1(3).
ICRP, 1994. Human respiratory tract model for radiological protection. ICRP Publication 66. Ann. ICRP 24(1–3).
ICRP, 2002. Basic anatomical and physiological data for use in radiological protection reference values. ICRP Publication 89. Ann. ICRP 32(3/4).
ICRP, 2006. Human alimentary tract model for radiological protection. ICRP Publication 100. Ann. ICRP 36(1/2).
ICRP, 2007. The 2007 Recommendations of the International Commission on Radiological Protection. ICRP Publication 103. Ann. ICRP 37(2–4).
ICRP, 2009. Adult reference computational phantoms. ICRP Publication 110. Ann. ICRP 39(2).
ICRP, 2010. Conversion coefficients for radiological protection quantities for external radiation exposures. ICRP Publication 116, Ann. ICRP 40(2–5).
ICRP, 2015. Occupational intakes of radionuclides: Part 1. ICRP Publication 130. Ann. ICRP 44(2).
ICRP, 2016. Computational framework for internal dose assessment for reference adults: specific absorbed fractions. ICRP Publication 133. Ann. ICRP 45(2).
ICRP, 2017. Occupational intakes of radionuclides: Part 2. ICRP Publication 134. Ann. ICRP 45(3/4).
Kim, C.H., Jeong, J.H., Bolch, W.E., et al., 2011. A polygon-surface reference Korean male phantom (PSRK-Man) and its direct implementation in Geant4 Monte Carlo simulation. Phys. Med. Biol. 56, 3137–3161.
Kim, C.H, Yeom, Y.S., Nguyen, T.T., et al., 2016. The reference phantoms: voxel vs polygon. Ann. ICRP 45(1S), 188–201.
Kim, H.S., Yeom, Y.S., Nguyen, T.T., et al., 2017. Inclusion of thin target and source regions in alimentary and respiratory tract systems of mesh-type ICRP adult reference phantoms. Phys. Med. Biol. 62, 2132–2152.
Kramer, R., Zankl, M., Williams, G., et al., 1982. The Calculation of Dose from External Photon Exposures Using Reference Human Phantoms and Monte-Carlo Methods. Pt. 1. No. GSF-S-885. Gesellschaft fuer Strahlen und Umweltforschung mbH, Muenchen.
Kramer, R., Khoury, H., Vieira, J., et al., 2006. MAX06 and FAX06: update of two adult human phantoms for radiation protection dosimetry. Phys. Med. Biol. 51, 3331–3346.
Lee, C., Lodwick, D., Hasenauer, D., et al., 2007. Hybrid computational phantoms of the male and female newborn patient: NURBS-based whole-body models. Phys. Med. Biol. 52, 3309–3333.
Lee, C., Lodwick, D., Hurtado, J., et al., 2010. The UF family of reference hybrid phantoms for computational radiation dosimetry. Phys. Med. Biol. 55, 339–363.
Lee, C., Lamart, S., Moroz, B.E., 2013. Computational lymphatic node models in pediatric and adult hybrid phantoms for radiation dosimetry. Phys. Med. Biol. 58, N59–N82.
Martz, R., 2012. The MCNP6 Book on Unstructured Mesh Geometry: User's Guide. Los Alamos National Laboratory, Los Alamos, NM.
Nguyen, T.T., Yeom, Y.S., Kim, H.S., et al., 2015. Incorporation of detailed eye model into polygon-mesh versions of ICRP-110 reference phantoms. Phys. Med. Biol. 60, 8695–8707.
Sato, T., Niita, K., Matsuda, N., et al., 2013. Particle and heavy ion transport code system, PHITS, Version 2.52. J. Nucl. Sci. Technol. 50, 913–923.
Si, H., 2015. Tetgen, a Delaunay-based quality tetrahedral mesh generator. ACM Trans. Math. Soft. 41, 2–11.

Tawhai, M.H., Pullan, A., Hunter, P., 2000. Generation of an anatomically based three-dimensional model of the conducting airways. Ann. Biomed. Eng. 28, 793–802.

Yeom, Y.S., Han, M.C., Kim, C.H., et al., 2013. Conversion of ICRP male reference phantom to polygon-surface phantom. Phys. Med. Biol. 58, 6985–7007.

Yeom, Y.S., Jeong, J.H., Han, M.C., et al., 2014. Tetrahedral-mesh-based computational human phantom for fast Monte Carlo dose calculations. Phys. Med. Biol. 59, 3173–3185.

Yeom, Y.S., Kim, H.S., Nguyen, T.T., et al., 2016a. New small-intestine modeling method for surface-based computational human phantoms. J. Radiol. Protect. 36, 230–245.

Yeom, Y.S., Wang, Z.J., Nguyen, T.T., et al., 2016b. Development of skeletal system for mesh-type ICRP reference adult phantoms. Phys. Med. Biol. 61, 7054–7073.

Zankl, M., Becker, J., Fill, U., et al., 2005. GSF Male and Female Adult Voxel Models Representing ICRP Reference Man – the Present Status. The Monte Carlo Method: Versatility Unbounded in a Dynamic Computing World. 17–21 April 2005, American Nuclear Society, LaGrange Park, IL, USA.

Zhang, J., Na, Y.H., Caracappa, P.F., et al., 2009. RPI-AM and RPI-AF, a pair of mesh-based, size-adjustable adult male and female computational phantoms using ICRP-89 parameters and their calculations for organ doses from monoenergetic photon beams. Phys. Med. Biol. 54, 5885–5908.